RSC Advances

PAPER

View Article Online
View Journal | View Issue

Cite this: *RSC Adv.*, 2017, **7**, 4092

Improved giant dielectric properties of $CaCu_3Ti_4O_{12}$ *via* simultaneously tuning the electrical properties of grains and grain boundaries by F^- substitution

Jutapol Jumpatam,[a] Bundit Putasaeng,[b] Narong Chanlek,[c] Pinit Kidkhunthod,[c] Prasit Thongbai,*[d] Santi Maensiri[e] and Prinya Chindaprasirt[f]

Received 26th November 2016
Accepted 23rd December 2016

DOI: 10.1039/c6ra27381e

www.rsc.org/advances

A novel concept to simultaneously modify the electric responses of the grain and grain boundaries of $CaCu_3Ti_4O_{12}$ ceramics was proposed, involving doping with F^- anions to improve the giant dielectric properties. The grain growth rate of $CaCu_3Ti_4O_{12}$ ceramics was enhanced by doping with F^- anions, which were found to be homogeneously dispersed in the microstructure. Substitution of F^- anions can cause an increase in the resistance of the insulating grain boundary and a decrease in the grain resistance. The former originated from the ability of the F^- dopant to enhance the Schottky barrier height at the grain boundaries, leading to a great decrease in the dielectric loss tangent by a factor of 5 ($\tan\delta < 0.1$). The latter was primarily attributed to the increase in Ti^{3+} and Cu^+ concentrations due to charge compensation, resulting in a significantly enhanced intensity of space charge polarization at the grain boundaries. This is the primary cause of the increase in dielectric permittivity from $\approx 10^4$ to $\approx 10^5$. The giant dielectric and electrical properties were well described by the Maxwell–Wagner polarization relaxation based on the internal barrier layer capacitor model of Schottky barriers at the grain boundaries.

1. Introduction

Recently, oxide materials with giant dielectric permittivity have found an important role in microelectronic devices and high-density storage applications such as capacitors and memory devices.[1–4] One of the most interesting giant dielectric materials is $CaCu_3Ti_4O_{12}$ (CCTO) ceramics. CCTO exhibited giant dielectric permittivity ($\varepsilon' > 10^4$ at 1 kHz) over a wide temperature range from 100 to 600 K.[5] The ε' value of CCTO ceramics was also weakly dependent on frequency in the radio frequency range. Unfortunately, the loss tangent ($\tan\delta$) of CCTO was still too large for practical applications in ceramic capacitors.[6–19]

Even now, the origin of giant dielectric response is still open to scientific debate. Most research groups believe that the extrinsic origin of the internal barrier layer capacitance (IBLC) mechanism at grain boundaries (GBs) is the primary cause of the giant dielectric response in CCTO ceramics.[12,14,20–23] According to the IBLC mechanism, the giant dielectric response in a polycrystalline ceramic is driven by its electrically heterogeneous microstructure. This special microstructure can be fabricated using a one-step processing method that forms insulating GBs sandwiched between n-type semiconducting grains. The electrical responses of the grain and GB can have a remarkable influence on the dielectric properties of CCTO ceramics.[12,13,15,22] Moreover, due to the existence of this special microstructure, CCTO ceramics can also exhibit the non-ohmic properties (or nonlinear current density–electric field, *J*–*E*).[24,25] This special behavior is believed to originate from the existence of an intrinsic potential barrier (*i.e.*, Schottky barrier) at GBs.[20] The presence of an electrostatic barrier at the GBs of CCTO ceramic was clearly confirmed using Kervin probe force microscopy.[24]

To improve the dielectric properties of CCTO ceramics, most investigations have focused on substitution of one of several doping cations into CCTO ceramics to tune the electrical properties of the grains and GBs. It has been widely demonstrated that enhancement of the GB resistance (R_{gb}) can reduce the low-frequency $\tan\delta$ value.[15,23,26] According to the space

[a]*Materials Science and Nanotechnology Program, Faculty of Science, Khon Kaen University, Khon Kaen 40002, Thailand*

[b]*National Metal and Materials Technology Center, National Science and Technology Development Agency, Thailand Science Park, Pathumthani 12120, Thailand*

[c]*Synchrotron Light Research Institute (Public Organization), 111 University Avenue, Muang District, Nakhon Ratchasima 30000, Thailand*

[d]*Integrated Nanotechnology Research Center (INRC), Department of Physics, Faculty of Science, Khon Kaen University, Khon Kaen 40002, Thailand. E-mail: pthongbai@kku.ac.th; Fax: +66 43 202374; Tel: +66 84 4190266*

[e]*Institute of Science, School of Physics, Suranaree University of Technology, Nakhon Ratchasima 30000, Thailand*

[f]*Sustainable Infrastructure Research and Development Center, Department of Civil Engineering, Faculty of Engineering, Khon Kaen University, Khon Kaen 40002, Thailand*

charge polarization theory (or interfacial polarization), an increase in mobile charges inside the semiconducting grains can lead to the possibility of accumulating free charges at the interface of insulating layers. This gives rise to a stronger intensity of the polarization at internal insulating interfaces, leading to an increase in ε'. The giant dielectric properties of CCTO ceramics were first reported by Subramanian *et al.*[6] There are further several reports of dopant cations substituted into CCTO ceramic such as Sr^{2+},[23] La^{3+},[7] Ni^{2+},[27] Mg^{2+},[9,28–30] Zn^{2+},[31,32] Ga^{3+},[14] Zr^{4+},[33,34] Sn^{4+},[11] Nb^{5+},[8] Ta^{5+} (ref. 12) and W^{6+}.[13,35] Substitution of many cations into Ca^{2+}, Cu^{2+} and Ti^{4+} sites in CCTO ceramics have significant effects on the values of their ε', tan δ, electrical conductivity of the GBs (σ_{gb}) and activation energies at the GBs (E_{gb}) and inside the grain (E_g). Usually, most of these dopants can be successfully used to improve a particular dielectric property (*e.g.*, to reduce tan δ or enhance ε'), while they simultaneously worsen other important dielectric properties of these materials. For example, substitution of higher cations into Ti^{4+} sites would increase free charges inside the semiconducting grains due to the excess electron of a dopant (*e.g.*, Nb^{5+} or Ta^{5+}). This can cause an increase in ε', which resulted from the enhanced space charges at the insulating interfaces. Unfortunately, it also causes a large decrease in R_{gb}, leading to a significant increase in a low-frequency tan δ.[8,12] Alternatively, doping CCTO with Mg^{2+} into Cu^{2+} sites can decrease tan δ However, the ε' value of Mg-doped CCTO was also decreased due to the decrease in free charges inside the grains, considering by the increase in R_g.[9,36]

It is expected that doping CCTO with an anion can increase free charges inside the grains due to charge compensation. Substitution of F^- into O^{2-} sites is electrically compensated by reduction of valance state of Ti^{4+} to Ti^{3+} and Cu^{2+} to Cu^+. It was clearly demonstrated that filling oxygen vacancies at the GBs can strongly increase the R_{gb} value by annealing in an O_2 atmosphere.[15,20,37] Alternatively, R_{gb} can be reduced by creating the oxygen vacancies at the grain boundaries *via* annealing in a N_2 atmosphere. Thus, it is also expected that substitution of F^- anions may have no effect on the insulating properties of the GBs because oxygen vacancies along the GBs are usually filled during cooling step of the sintering process. This also helps retain the insulating nature of the GBs. To the best our knowledge, there have been few reports of an anion dopant being substituted into CCTO ceramics.[38] The effects of an anion dopant on the microstructure and electrical properties of the grain and GB have never been reported.

In this work, a new strategy to improve the dielectric properties of CCTO ceramics was used by doping with F^- anions to modify the electrical responses of the grains and GBs. The effects of F^- anions on the microstructural evolution and associated dielectric properties were studied and discussed. As expected, doping CCTO ceramics with F^- anions at O^{2-} sites resulted in improved dielectric properties *via* a large enhancement of ε' and significant decrease in tan δ.

2. Experimental procedure

$CaCu_3Ti_4O_{12-x}F_x$ ceramics, where $x = 0$, 0.05, 0.1, and 0.2 (referred to as the CCTO, F05, F10 and F20 samples, respectively), were prepared using a solid state reaction method. The starting materials used were $CaCO_3$ (Aldrich, ≥99.0% purity), CuO (Merck, 99% purity), CuF_2 (Sigma-Aldrich, 99.9% purity) and TiO_2 (Sigma-Aldrich, 99.9% purity). First, a stoichiometric mixture of the starting materials for each composition was mixed by ball milling using zirconia (ZrO_2) media in ethanol for 12 h. Second, the mixed slurries were dried and calcined at 900 °C for 15 h. Then, the calcined powders were ground and pressed into pellets with 9.5 mm in diameter and 1–2 mm in thickness by a uniaxial compression at 200 MPa. Finally, these pellets were sintered in air at 1075 °C for 3 h.

The phase composition and crystal structure were characterized using X-ray diffraction (XRD; PANanalytical EMPYREAN). Rietveld quantitative phase analysis was done using the X'Pert High Score Plus v3.0e software package by PANalytical. The as-sintered ceramics were carefully polished to obtain smooth surfaces. The grain and GB structure of the polished-samples was formed by thermally etching at 1050 °C for 1 h. Surface morphologies of sintered ceramics were revealed using scanning electron microscopy (SEM; SEC, SNE-4500M). Elemental distribution of the F dopant atoms and the major elements (*i.e.*, Ca, Cu, Ti, and O) in the sintered CCTO ceramics was examined using a field-emission scanning electron microscopy (FE-SEM) with energy-dispersive X-ray analysis (EDX) (HITACHI SU8030, Japan). X-ray Absorption Near Edge Structure (XANES) spectra were collected at the SUT-NANOTEC-SLRI XAS beamline (BL5.2) (using an electron energy of 1.2 GeV, a bending magnet, beam current of 80–150 mA, and 1.1 to 1.7 × 10^{11} photons per s) at the Synchrotron Light Research Institute (SLRI), Nakhon Ratchasima, Thailand. Details of this characterization technique have been published.[26] The normalized XANES data were processed and analyzed after background subtraction in the pre-edge and post-edge region using ATHENA software that is included in the IFEFFIT package.[39] The chemical states of Cu and Ti were analyzed using X-ray photoelectron spectroscopy (XPS), PHI5000 VersaProbe II, ULVAC-PHI, Japan) at the SUT-NANOTEC-SLRI Joint Research Facility, Synchrotron Light Research Institute (SLRI), Thailand. The XPS spectra were fitted using PHI MultiPak XPS software with a combination of Gaussian–Lorentzian lines.

Before electrical measurements, both surfaces of the sintered ceramics were polished until smooth, washed, and dried at 150 °C overnight. The polished samples were coated by sputtering Au on their surfaces for 8 min at 25 mA using a Polaron SC500 sputter coating unit. The dielectric properties were measured over the temperature range of −70 to 220 °C using a KEYSIGHT E4990A Impedance Analyzer in the frequency range of 10^2 to 10^7 Hz with an oscillation voltage of 0.5 V. Each measurement temperature was kept constant with a precision of ±0.1 °C. Nonlinear *J–E* properties at room temperature (RT) were determined using a high voltage measurement unit (Keithley Model 247). The breakdown

electric field (E_b) was achieved at $J = 1$ mA cm^{-2}. The nonlinear coefficient (α) was calculated using the following formula:

$$\alpha = \frac{\log(J_2/J_1)}{\log(E_2/E_1)} \quad (1)$$

where E_1 and E_2 are the applied electric fields, at $J_1 = 1$ and $J_2 = 10$ mA cm^{-2}, respectively.

3. Results and discussion

The crystal structure and phase composition of all the sintered ceramic samples were studied. Fig. 1 shows the Rietveld refinement profile fits of the XRD patterns for all the samples. The profile fits confirmed the formation of a single CCTO phase (JCPDS 75-2188) in the CCTO and all F$^-$-doped CCTO (CCTOF) ceramics. It was found that all the diffraction peaks were well indexed based on the bcc structure within space group $Im\bar{3}$. Impurities (*e.g.*, TiO_2, CuO, Cu_2O and $CaTiO_3$) were not seen in the profile fits. The lattice parameters (a) of all the samples are summarized in Table 1. The a values of all the samples can be compared to 7.391 Å for un-doped CCTO (JCPDS 75-2188). It is notable that the a values of CCTOF did not change with F$^-$ dopant concentration. This result is similar to that reported in previous work with $CaCu_3Ti_4O_{12-x}F_x$ where $x = 0$–0.2.[38] The unchanged lattice parameter was likely because the ionic radii of the substituted F$^-$ anion ($r_4 = 1.31$ Å) and the host O^{2-} ion ($r_4 = 1.38$ Å) are not greatly different.[40]

Surface morphologies of the CCTO and CCTOF ceramics sintered at 1075 °C for 3 h are shown in Fig. 2. As can be clearly seen, there was abnormal grain growth in the microstructure of the CCTO ceramic, where the large sized grains (≈30–50 μm) were surrounded by small grains (≈5–10 μm). This is generally reported in literature and was ascribed to the liquid phase sintering mechanism.[14,26,32] It was found that the mean grain size of CCTO ceramics was greatly enlarged by doping with F$^-$ anions. Almost all grains of the F05, F10 and F20 samples were very large (≈40–100 μm).

Usually, the grain growth mechanism of a polycrystalline ceramic is associated with mass transport by diffusion of ions (or atoms) across the GB layer. During sintering, the dopant directly melts and/or reacts with a small part of the major phase to form a eutectic liquid. These can cause a formation of a liquid phase in the microstructure. The liquid was present at the contact areas between the particles in the ceramic microstructure. This can contribute to promotion of the diffusion of ions. For polycrystalline ceramics, a liquid phase generally originates from a eutectic liquid. The eutectic temperature for

Table 1 Lattice parameter (a), dielectric permittivity (ε') and loss tangent (tan δ) at RT and 1 kHz, conduction activation energies of the grain (E_g) and grain boundary (E_{gb}), nonlinear coefficient (α) and nonlinear breakdown electric field (E_b)

Samples	a (Å)	ε'	tan δ	E_g	E_{gb}	α	E_b
CCTO	7.393(2)	23 263	0.145	0.083	0.630	3.77	308.1
F05	7.393(9)	69 732	0.098	0.091	0.696	3.57	345.5
F10	7.392(7)	81 306	0.077	0.091	0.714	3.58	331.5
F20	7.393(8)	98 396	0.087	0.116	0.739	4.18	345.8

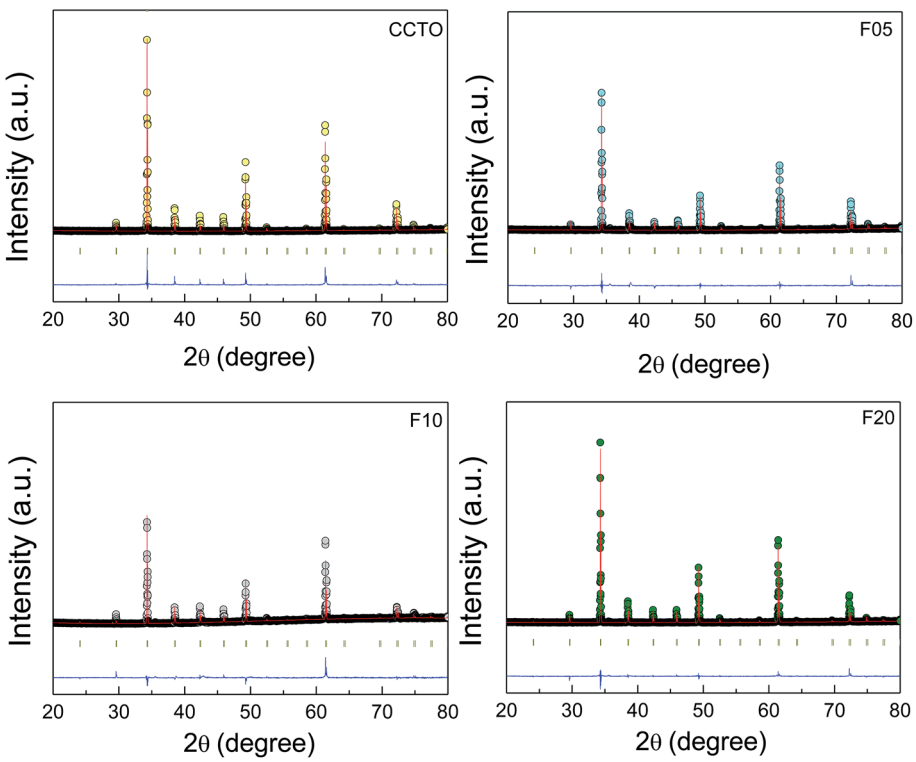

Fig. 1 Profile fits for the Rietveld refinements of the XRD patterns of CCTO, F05, F10 and F20 samples.

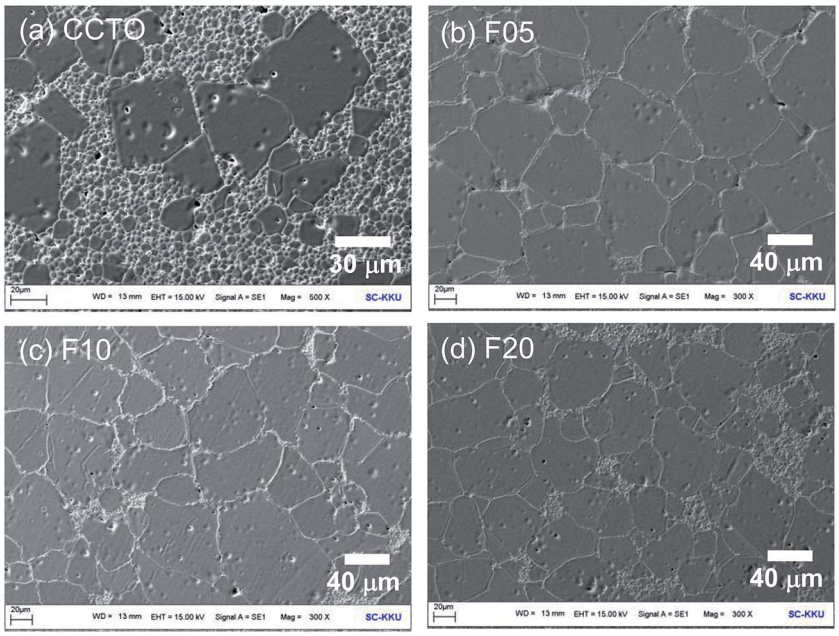

Fig. 2 SEM images of polished surfaces of (a) CCTO, (b) F05, (c) F10 and (d) F20 samples.

$CuO–TiO_2$ is about 950 °C for CCTO ceramics.[35] Although the liquid phase formed by melting of the dopant usually occurs in metallic systems, it is also possible in CCTOF ceramics. This is due to the low melting point of CuF_2 (836 °C). Thus, the formation of a liquid phase is likely caused by these two mechanisms. Enhancement of GB mobility resulted from the presence of the liquid phase(s) and was suggested an important factor for increasing grain growth rate in CCTOF ceramics.

Fig. 3 shows the SEM mapping images of the F05 sample. This result confirms the existence of all major elements (*i.e.*, Ca, Cu, Ti, and O) and confirms the homogeneous dispersion of F^- dopant in both of the grains and GBs. Segregation of the F^- dopant in any specific region was not seen. In contrast, segregation of Cu was observed along the GBs, which is also generally reported in previous studies.[22] This result strongly confirms that the liquid phase is closely associated with a Cu-rich phase, which likely originated from melting of CuF_2 and the eutectic phase of $CuO–TiO_2$.

The frequency dependence of the dielectric properties of all the ceramic samples is shown in Fig. 4 ε' was slightly dependent on frequency in the range of 10^2 to 10^5 Hz. Notably, ε' can be enhanced from $\approx 10^4$ to $\approx 10^5$ by doping with F^- anions. Considering the microstructural change in CCTOF ceramics, the enlarged grain size is one of the most important parameters that increased ε'. However, the linear and continuous increase in ε' of the F^--doped CCTO ceramics was not correlated with their grain sizes. ε' increased with increasing anion dopant concentration, but not for the mean grain sizes. Therefore, variation in ε' cannot be attributed to the change in the microstructure only. As illustrated in the inset of Fig. 4, a low-frequency tan δ of CCTO ceramics was greatly decreased by doping with F^- anions. At 10^2 Hz, the tan δ of the CCTOF

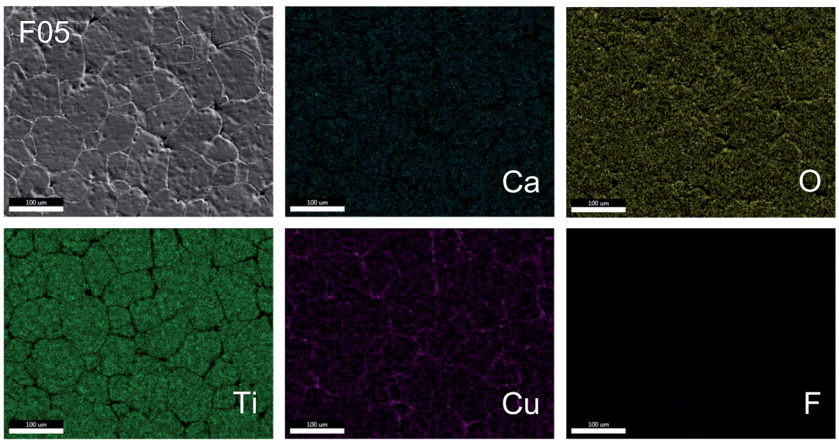

Fig. 3 Element mapping of the F05 sample for Ca, Cu, Ti, O and F.

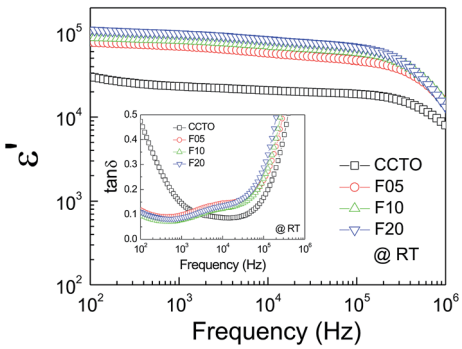

Fig. 4 Frequency dependency of dielectric permittivity (ε') at RT for CCTO, F05, F10 and F20 samples; inset show the loss tangent (tan δ) as a function of frequency at RT.

ceramics was reduced by a factor of 5. At frequencies higher than 10^5 Hz, the frequency dependent behaviors of tan δ for all of the samples were similar, *i.e.*, tan δ increased with increasing frequency. This indicates the dielectric relaxation behavior of primary polarization, which will be discussed below. The ε' and tan δ values at RT and 1 kHz of all the ceramic samples are summarized in Table 1. It is notable that the low-frequency tan δ of the CCTOF ceramics was significantly reduced to <0.1, while ε' greatly increased. Generally, this result is hard to achieve in CCTO ceramics because variations in tan δ and ε' values are usually directly proportional. The ε' and tan δ values of the CCTO and CCTOF ceramics compared to those reported in literature for both of un-doped and metal ions-doped CCTO ceramics prepared by using different method and sintered under various conditions are shown in Table 2.

The dielectric relaxation behavior of CCTO and CCTOF ceramics was studied. As shown in Fig. 5, two dielectric relaxations were observed in distinct frequency ranges. The low-frequency dielectric relaxation likely originated from the sample-electrode effect.[41] The relatively high-frequency dielectric relaxation (*i.e.*, the primary relaxation) has widely been accepted as associated with the IBLC effect, *i.e.*, the Maxwell–Wagner polarization relaxation.[13,21] The step-like decrease in ε' and relaxation peak of ε'' (ε'' is the imaginary part of the complex dielectric permittivity or dielectric loss, $\varepsilon'' = \varepsilon' \times \tan\delta$) shifted to a higher frequency with increasing temperature, indicating a thermally activated relaxation mechanism. The activation energy for dielectric relaxation can be calculated from the critical frequency (f_{max}) at various temperatures at which the relaxation peak appeared as:

$$f_{max} = f_0 \exp\left(\frac{-E_a}{k_B T}\right), \quad (2)$$

where f_0 is the pre-factor, E_a is the activation energy required for relaxation process, T is absolute temperature and k_B is Boltzmann constant. The frequency dependence of f_{max} for all the samples obeyed the Arrhenius law in eqn (2), inset of Fig. 5(d). The E_a values of the CCTO, F05, F10 and F20 samples were about 0.096, 0.096, 0.099 and 0.115 eV, respectively. These values are comparable to the reported values of 0.103 eV,[32] 0.011 eV (ref. 11) and 0.101 eV.[28] Doping CCTO with F^- anions into O^{2-} sites has a small influence on the dielectric-relaxation activation energy of CCTO ceramics.

To elucidate the influences of F^- anion dopant ions on the dielectric properties of CCTO ceramics, the grain and GB responses were studied using an impedance spectroscopy technique. Fig. 6(a) and (b) show Z^* plots for all the samples at RT and 80 °C, respectively. Only the linear part of the semicircular arcs was observed at RT in the frequency range of 10^2 to 10^6 Hz. A nonzero intercept on the Z' axis was observed, inset of Fig. 6(a), indicating an electrical response of the semiconducting grains.[42,43] Thus, the linear part of the semicircular arcs should be due to the electrical response of the GBs. The grain resistance (R_g) values (estimated from the nonzero intercept) of the CCTOF ceramics were smaller than that of the undoped CCTO ceramic by a factor of 2. At RT, R_g of the CCTO sample was ≈100 Ω cm, while R_g values of the CCTOF ceramics were nearly the same in value with $R_g \approx 50$ Ω cm. At RT, it is very difficult (or perhaps impossible) to accurately calculate the value of R_{gb} in the measured frequency range since just few data points on the full arcs appeared in these Z^* plots. The trend of R_{gb} values for the CCTOF ceramics cannot be determined. To obtain this, a Z^* plot at a high temperature should be performed. In Fig. 7(b), the R_{gb} of each sample was estimated and

Table 2 Dielectric permittivity (ε') and loss tangent (tan δ) at RT and 1 kHz of un-doped CCTO and metal ion-doped CCTO ceramics doping with different ions

Doped-CCTO ceramics (preparation method)	Sintering condition	ε'	tan δ
Ni-Doped CCTO (SSR method)[44]	1040 °C/4 h	69 833	0.073
Sn-Doped CCTO (SSR method)[44]	1040 °C/4 h	51 443	0.061
Si-Doped CCTO (SSR method)[44]	1040 °C/4 h	55 240	0.136
Al-Doped CCTO (SSR method)[44]	1040 °C/4 h	30 226	0.100
Un-doped CCTO (SSR method)[44]	1040 °C/4 h	45 972	0.109
Un-doped CCTO (sol–gel method)[16]	1060 °C/48 h	~42 250	~0.15
Un-doped CCTO (SSR method)[17]	1060 °C/48 h	~100 000	~1.0
Un-doped CCTO (molten salt method)[19]	1060 °C/1 h	~10 000	~0.15
	1060 °C/3 h	~10 000	~0.15
Un-doped CCTO (SSR method with quenching in water)[18]	1060 °C/3 h	~17 500	~0.085
Un-doped CCTO (SSR method) [in this work]	1075 °C for 3 h	23 263	0.145
$CaCu_3Ti_4O_{11.9}F_{0.10}$ (SSR method) [in this work]	1075 °C for 3 h	81 306	0.077

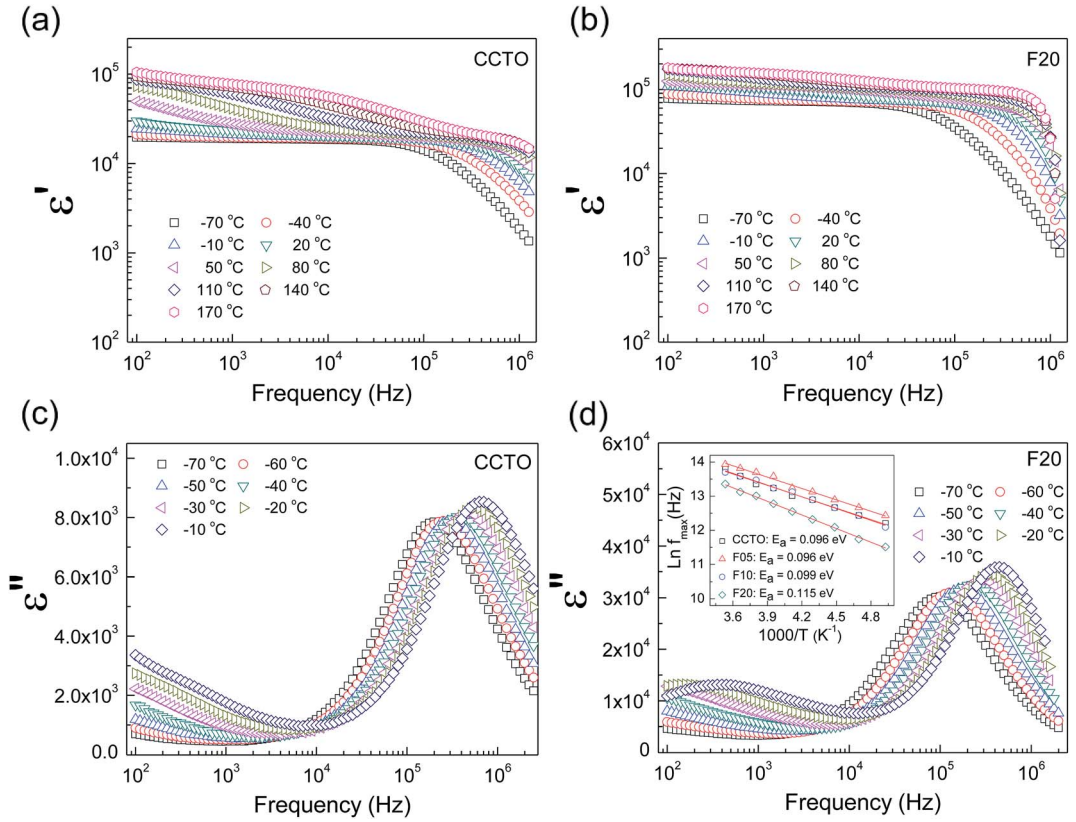

Fig. 5 Frequency dependencies of dielectric permittivity (ε') and dielectric loss (ε'') at various temperatures for (a, c) CCTO and (b, d) F20 samples; inset of (d) shows Arrhenius plots of f_{max} for the dielectric relation.

found to be significantly increased by doping with F^-. R_{gb} of the CCTOF ceramics was enhanced even through the mean grain size increased compared to that of the CCTO sample. This result gives a significant clue, reflecting the largely enhanced resistance of individual GB layers. This is one of the most important factors contributing to reduction in a low-frequency tan δ in CCTOF ceramics [inset of Fig. 4]. Thus, the distribution of dopants near GBs can cause an increase in the GB resistivity, which often make great influence on the low-frequency dielectric properties,[44] as clearly seen in Fig. 5. It is worth noting that all the samples were electrically heterogeneous, consisting of grains with very small R_g values and very high values of R_{gb}. Therefore, it is reasonable to suggest that the giant dielectric response in CCTOF ceramics originated from the IBLC effect.

R_g and R_{gb} values can be calculated in various temperatures. The conductivities of the grain (σ_g) and GB (σ_{gb}) were calculated from R_g and R_{gb}, respectively. As demonstrated in Fig. 6(c) and (d), the temperature dependencies of σ_g and σ_{gb} follow the Arrhenius law:

$$\sigma_{g/gb} = \sigma_0 \exp\left(\frac{-E_{g/gb}}{k_B T}\right), \quad (3)$$

where σ_0 is a constant value and E_g and E_{gb} are the conduction activation energies inside the grains and GBs, respectively. The E_{gb} values of the CCTO, F05, F10 and F20 samples were about 0.630, 0.696, 0.714 and 0.739 eV, respectively. The E_g values for all the samples are summarized in Table 1. E_g slightly increased with increasing F^- dopant concentration. It was observed that the trends of variation in E_g and E_a values were similar. According to the Maxwell–Wagner polarization relaxation model, the temperature dependence at the critical frequency, f_{max}, of a thermally activated relaxation process can be expressed in term of R_g, as the following:[13,21]

$$f_{max} \approx (2\pi R_g C_{gb})^{-1} \approx (2\pi C_{gb})\left(R_g^0\right)^{-1} \exp\left(\frac{-E_g}{k_B T}\right), \quad (4)$$

where C_{gb} is the capacitance of GBs. From eqn (2), the temperature dependence of f_{max} for the dielectric relaxation process in CCTO and CCTOF ceramics follows the temperature dependence of the conduction process of the grains, since C_{gb} is nearly independent of temperature. According to eqn (2)–(4), the activation energies required for electrical conduction in the grain interiors and for dielectric relaxation process should be the very close. Thus, the calculated E_a and E_g values strongly confirm that the giant dielectric response in CCTOF ceramics can be attributed to the Maxwell–Wagner polarization based on the IBLC structural model.

As shown in the inset of Fig. 6(a), R_g of CCTO ceramics was reduced by doping with F^- anions, indicating an increase in the concentration of free charge carriers in the grain interiors. To clarify the effect of F^- doping on the electrical properties of the grains, variation in valence states of Cu^{2+} and Ti^{4+} ions in CCTO

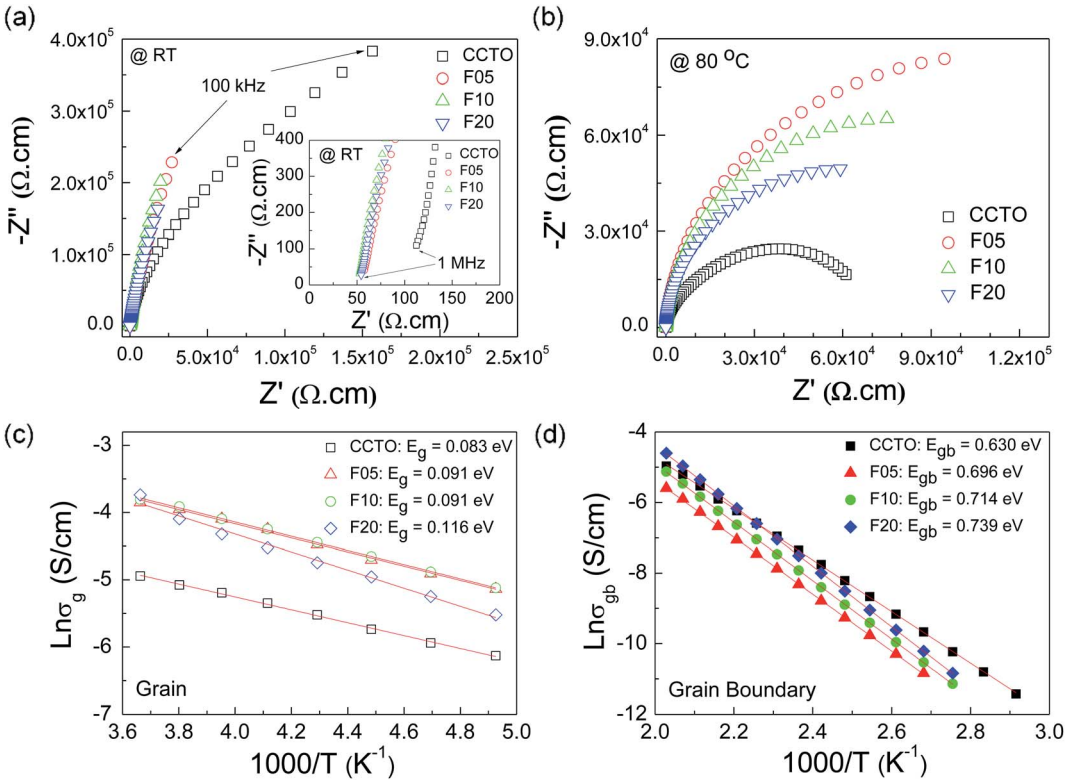

Fig. 6 (a and b) Impedance complex plane (Z^*) plots of CCTO, F05, F10 and F20 samples at room temperature and 80 °C, respectively; inset of (a) shows an expanded view of high frequency Z^* plots at RT, revealing the nonzero intercept on Z' axis. (c and d) Arrhenius plots of σ_g and σ_{gb}, respectively.

and CCTOF samples was investigated using XPS and XANES techniques. As illustrated in Fig. 7(a) and (c), the main XPS peaks at ≈933 eV for the CCTO and F10 samples confirm the existence of large numbers of Cu^{2+} ions.[9,28,32] The Cu $2p_{3/2}$ region can be divided into three peaks using Gaussian–Lorentzian profile fitting. The small XPS peaks at relatively lower and higher binding energies at ≈931 and ≈936 eV indicated the existence of Cu^{+} and Cu^{3+}, respectively.[9,28,32] The Cu^{+}/Cu^{2+} ratios of the CCTO and F10 samples were, respectively, about 4.26% and 5.65%, while their respective Cu^{3+}/Cu^{2+} ratios were 13.62% and 27.22%. Doping CCTO with F^{-} caused an increase in both Cu^{+} and Cu^{3+} concentrations.

In addition to Cu^{+} and Cu^{3+}, the presence of Ti^{3+} ions is usually considered a major cause of the formation of n-type semiconducting grains in CCTO ceramics. As depicted in Fig. 7(b) and (d), the primary XPS peak at ≈458 eV for Ti^{4+} was confirmed in all the samples. Unfortunately, the presence of Ti^{3+} cannot be modeled using Gaussian–Lorentzian profile fitting. This may be due to a small amount of Ti^{3+} in both the samples.[2] Thus, XANES was used to further investigate to the existence of Ti^{3+}. Fig. 8 shows normalized Ti K-edge XANES spectra of the CCTO and F10 samples as well as the standard TiO_2 (Ti^{4+}) and Ti_2O_3 (Ti^{3+}) samples. It was found that the position of the edge energy of both samples was very close to the TiO_2 standard. As expected, a small amount of Ti^{3+} was confirmed to exist. To obtain the ratios of Ti^{3+}/Ti^{4+}, the edge value was calculated from the maximum value of the first derivative in the edge region.[15] The ratio of Ti^{3+}/Ti^{4+} can be calculated from the energy edge value.[39] The ratios of Ti^{3+}/Ti^{4+} in the CCTO and F10 samples were found to be 0.82% and 2.46%, respectively.

Substitution of O^{2-} with F^{-} anions requires charge compensation, which can be achieved by reduction in cation valence ($Cu^{2+} \rightarrow Cu^{+}$ and $Ti^{4+} \rightarrow Ti^{3+}$). This charge compensation behavior is similar to that observed in the case of Y^{3+} doped-CCTO ceramics, which R_g of CCTO was reduced by doping with Y^{3+}.[45,46] It is worth noting that the Cu^{3+}/Cu^{2+} ratio of the F10 sample was significantly increased. As shown in the SEM-mapping image for Cu dispersion, Fig. 3, segregation of Cu-rich phase along the GBs was observed. This indicated the decomposition of CuO from the CCTO lattice, creating cation vacancies. Therefore, it is possible that the increased Cu^{3+}/Cu^{2+} ratio of the F10 sample might be due to the creation of Cu vacancies.[9]

Generally, the conductivity of n-type semiconducting grains is elevated by increasing the number of free electrons. Thus, the reduction in R_g of the CCTOF samples should be correlated with the increase in Cu^{+}/Cu^{2+} and Ti^{3+}/Ti^{4+} ratios over those found in the CCTO sample. For p-type semiconductor CuO ceramics, conduction is primarily caused by hole hopping between $Cu^{3+} \leftrightarrow Cu^{2+}$. The increase in the Cu^{3+}/Cu^{2+} ratio may also be an important cause of the reduced R_g. Form this point of view, hopping of charge carriers between $Cu^{+} \leftrightarrow Cu^{2+}$, $Cu^{3+} \leftrightarrow Cu^{2+}$, and $Ti^{3+} \leftrightarrow Ti^{4+}$ sites in the CCTO structure can result in

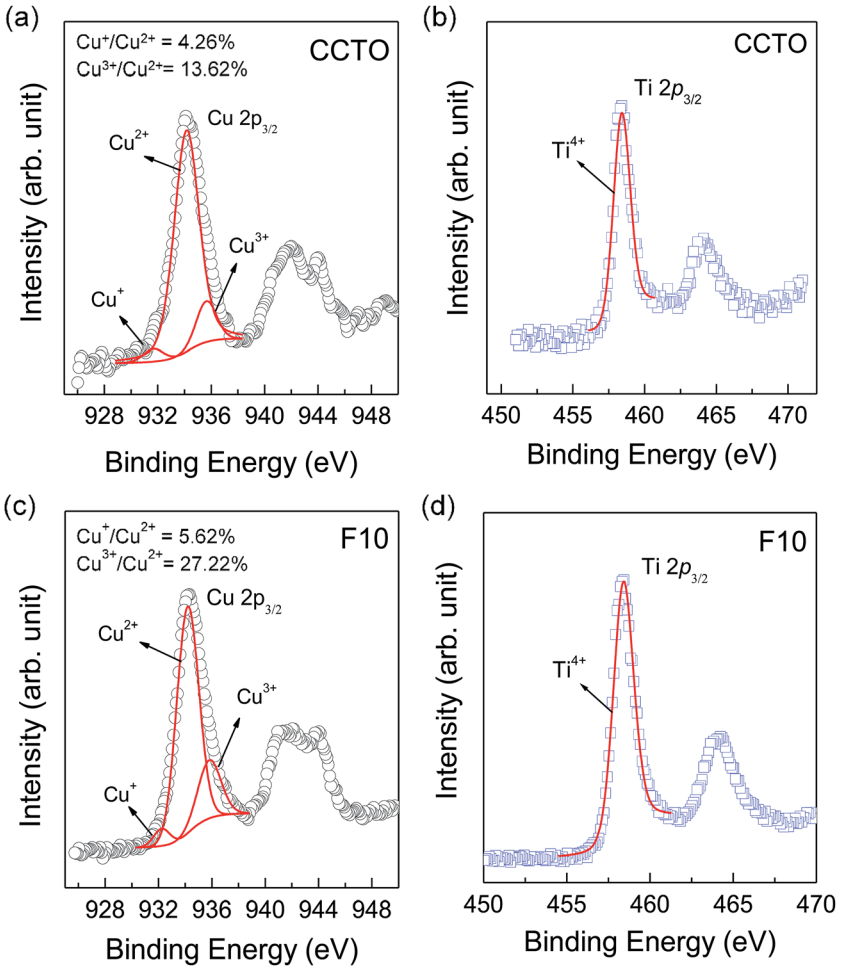

Fig. 7 XPS spectra of CCTO and F10 samples: (a, c) Ti 2p regions and (b, d) Cu 2p regions.

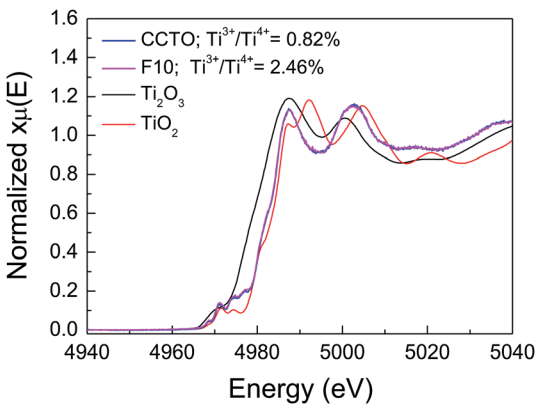

Fig. 8 Normalized X-ray absorption near edge structure (XANES) spectra for Ti K-edge of the CCTO and F10 samples.

electrical conductivity. According to our previous report, we found that the variation in R_g of $Na_{0.5}Y_{0.5}Cu_3Ti_4O_{12}$ ceramics was only consistent with a change in the Ti^{3+}/Ti^{4+} ratio, whereas changes in Cu^+/Cu^{2+} and Cu^{3+}/Cu^{2+} ratios was not correlated to R_g values.[47] The conduction mechanism inside the n-type semiconducting grains might be primarily attributed to electron hopping from a Ti^{3+}–O–Ti^{4+} to a Ti^{4+}–O–Ti^{3+}. Hopping of charge carriers between complex defects, *i.e.*, Cu^+–O–Cu^{2+} ↔ Cu^{2+}–O–Cu^{3+}, was likely difficult owing to much different valance states of Cu^+ and Cu^{3+}.

The effect of F^- anions on the non-ohmic properties of CCTO ceramics is illustrated in Fig. 9. All the samples exhibited nonlinear *J–E* characteristics. Accordingly, E_b and α values were calculated and summarized in Table 1. According to the improved dielectric properties and the observed nonlinear electrical properties of CCTOF ceramics, it was suggested that the sample could be applied as capacitor-varistors.[48] α values for all the samples were not significantly different, while E_b values of the CCTOF samples were greater than that of the undoped CCTO sample, even though their grain sizes were larger than those of the CCTO sample. The volume fraction of the GB, which is inversely proportional to its mean grain size, was decreased by doping with F^- anions. The increase in E_b of the CCTOF samples was consistent with their enhanced R_{gb} values over that of the CCTO sample. Although the volume fraction of the GB in the CCTOF samples was lower than that of the CCTO sample, the total resistance of their GBs (R_{gb}) and E_b were larger.

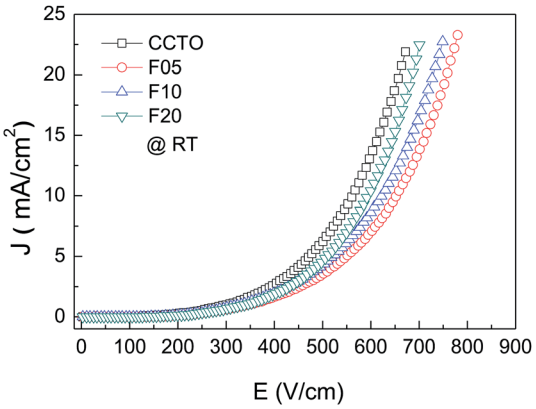

Fig. 9 Nonlinear current density–electric field (J–E) characteristics at RT of CCTO, F05, F10 and F20 samples.

Thus, the resistivity of an individual GB layer of the CCTOF samples should much be larger than that of the CCTO sample. These results indicate that the intrinsic property (*i.e.*, potential barrier height) of the GB of CCTO ceramics was enhanced by F^- doping. It was reasonably proposed that based on the n-type semiconducting grains of CCTO ceramics, the electronic energy band structure across the GB layer was equivalent to n–i–n.[20,49] Double Schottky potential barriers can be created at interfaces between n-type grains caused by trapping at acceptor states. This resulted in the bending of the conduction band across the GB. A potential barrier (Φ_B) was created at the GB sandwiched by n-type semiconducting grains.[20] In the absence of a DC bias, Φ_B can be expressed as:

$$\Phi_B = \frac{qN_s^2}{8\varepsilon_0\varepsilon' N_d}, \quad (5)$$

where N_s is the acceptor (surface charge) concentration, ε' is the relative permittivity of materials, N_d is the charge carrier concentration in the semiconducting grains and q is the electronic charge. It was reported that the activation energy for conduction at the GBs has a close relationship with the potential barrier height at the GBs.[10,20] E_{gb} and Φ_B were nearly the same in value. As shown in Fig. 6(d) and Table 1, the enhanced E_{gb} values indicated an increase in Φ_B. As demonstrated in the inset of Fig. 6(a), R_g (or σ_g) of all the CCTOF samples was smaller than that of the CCTO sample, indicating that the charge carrier concentration in the semiconducting grains (N_d) of the CCTOF samples was higher. This is responsible for the observed increase in the potential barrier height at the GBs in the CCTOF ceramic samples. Generally, it was observed that the mechanism of potential barrier formation in CCTO ceramics was also correlated with oxygen enrichment at the GBs.[25] For this point of view, it was proposed that the GB region may possess a p-type semiconductor nature, resulting from high oxygen content and/or vacancies of metal ions along the GBs compared with the n-type semiconductor nature inside the grains.[50] For CCTOF ceramics, the creation of oxygen vacancies may possibly be inhibited (or decreased) by F^- doping anions due to the lower valence state of the dopant, retaining the p-type semiconductor nature of the GBs and potential barrier height. Thus, substitution of F^- anions not only decreased the possibility of a reduction in Φ_B as a result of creation of oxygen vacancies, but it also enhanced Φ_B resulting from the creation of free charges inside the semiconducting grains.

Substitution of F^- anions into CCTO ceramics can simultaneously improve the electrical properties of the grains and GBs. These can cause increases in both of the free charge carrier concentration inside the semiconducting grains and Schottky barrier height at the GBs, respectively. Under an applied electric field, more charges accumulated at the interface between the semiconducting grain and GB layer due to a high concentration of free charges inside the grain producing a stronger intensity of interfacial polarization (Maxwell–Wagner polarization). This gave rise to a large increase in ε'. Enhanced Φ_B resulting in R_{gb} is the major cause the reduced low-frequency tan δ.

4. Conclusions

Significantly improved giant dielectric properties of CCTO ceramics *via* simultaneously tuning the electric properties of the grains and GBs was successfully done by doping CCTO with F^- anions. The grain size of CCTO ceramics was thus enlarged. The low-frequency tan δ of F^--doped CCTO ceramics was greatly reduced by a factor of 5 compared to that of the undoped CCTO ceramic, which was attributed to a large increase in R_{gb} and potential barrier height at the GBs. These results were confirmed by the slight increase in electric breakdown strength of F^--doped CCTO ceramics, even though the mean grain size was greatly increased. According to the XPS and XANES results, it was shown that the charge carrier concentration inside the semiconducting grains of F^--doped CCTO ceramics was increased corresponding to the observed reduction in R_g. This was responsible for the observed increase in ε' from $\approx 10^4$ to $\approx 10^5$ at 1 kHz due to the increased intensity of interfacial polarization at the GBs. Maxwell–Wagner polarization relaxation based on the internal barrier layer capacitor model of Schottky barriers at the GBs can be used to clearly explain the variations of the giant dielectric behavior and nonlinear electrical properties of F^--doped CCTO ceramics.

Acknowledgements

This work was financially supported by the Thailand Research Fund (TRF) and Khon Kaen University (Contract No. RSA5880012) and under the TRF Senior Research Scholar (Contract No. RTA5780004). The authors would like to thank the Synchrotron Light Research Institute (BL5.2) (Public Organization), Nakhon Ratchasima, Thailand for XANES measurements and the SUT-NANOTEC-SLRI Joint Research Facility for XPS facility. J. Jumpatam thanks the Thailand Research Fund under The Royal Golden Jubilee Ph.D. Program [Grant number PHD/0079/2557] for his Ph.D. scholarship.

References

1 C. C. Homes, T. Vogt, S. M. Shapiro, S. Wakimoto and A. P. Ramirez, *Science*, 2001, **293**, 673–676.

2 W. Hu, Y. Liu, R. L. Withers, T. J. Frankcombe, L. Norén, A. Snashall, M. Kitchin, P. Smith, B. Gong, H. Chen, J. Schiemer, F. Brink and J. Wong-Leung, *Nat. Mater.*, 2013, **12**, 821–826.
3 G. Liu, H. Fan, J. Xu, Z. Liu and Y. Zhao, *RSC Adv.*, 2016, **6**, 48708–48714.
4 W. Tuichai, S. Danwittayakul, S. Maensiri and P. Thongbai, *RSC Adv.*, 2016, **6**, 5582–5589.
5 A. O. Turky, M. M. Rashad, Z. I. Zaki, I. A. Ibrahim and M. Bechelany, *RSC Adv.*, 2015, **5**, 18767–18772.
6 M. A. Subramanian, D. Li, N. Duan, B. A. Reisner and A. W. Sleight, *J. Solid State Chem.*, 2000, **151**, 323–325.
7 B. Shri Prakash and K. B. R. Varma, *J. Mater. Sci.: Mater. Electron.*, 2006, **17**, 899–907.
8 S.-H. Hong, D.-Y. Kim, H.-M. Park and Y.-M. Kim, *J. Am. Ceram. Soc.*, 2007, **90**, 2118–2121.
9 M. Li, G. Cai, D. F. Zhang, W. Y. Wang, W. J. Wang and X. L. Chen, *J. Appl. Phys.*, 2008, **104**, 074107.
10 L. Liu, H. Fan, P. Fang and X. Chen, *Mater. Res. Bull.*, 2008, **43**, 1800–1807.
11 L. Ni, X. M. Chen and X. Q. Liu, *Mater. Chem. Phys.*, 2010, **124**, 982–986.
12 P. Thongbai, J. Jumpatam, T. Yamwong and S. Maensiri, *J. Eur. Ceram. Soc.*, 2012, **32**, 2423–2430.
13 P. Thongbai, J. Jumpatam, B. Putasaeng, T. Yamwong and S. Maensiri, *J. Appl. Phys.*, 2012, **112**, 114115.
14 J. Jumpatam, B. Putasaeng, T. Yamwong, P. Thongbai and S. Maensiri, *Ceram. Int.*, 2013, **39**, 1057–1064.
15 J. Boonlakhorn and P. Thongbai, *J. Electron. Mater.*, 2015, **44**, 3687–3695.
16 L. Liu, H. Fan, P. Fang and L. Jin, *Solid State Commun.*, 2007, **142**, 573–576.
17 L. Liu, H. Fan, X. Chen and P. Fang, *J. Alloys Compd.*, 2009, **469**, 529–534.
18 L. Liu, D. Shi, S. Zheng, Y. Huang, S. Wu, Y. Li, L. Fang and C. Hu, *Mater. Chem. Phys.*, 2013, **139**, 844–850.
19 Y. Huang, L. Liu, D. Shi, S. Wu, S. Zheng, L. Fang, C. Hu and B. Elouadi, *Ceram. Int.*, 2013, **39**, 6063–6068.
20 T. Adams, D. Sinclair and A. West, *Phys. Rev. B: Condens. Matter Mater. Phys.*, 2006, **73**, 094124.
21 J. Liu, C.-G. Duan, W.-G. Yin, W. Mei, R. Smith and J. Hardy, *Phys. Rev. B: Condens. Matter Mater. Phys.*, 2004, **70**, 144106.
22 R. Schmidt, M. C. Stennett, N. C. Hyatt, J. Pokorny, J. Prado-Gonjal, M. Li and D. C. Sinclair, *J. Eur. Ceram. Soc.*, 2012, **32**, 3313–3323.
23 Z. Yang, L. Zhang, X. Chao, L. Xiong and J. Liu, *J. Alloys Compd.*, 2011, **509**, 8716–8719.
24 S.-Y. Chung, I.-D. Kim and S.-J. L. Kang, *Nat. Mater.*, 2004, **3**, 774–778.
25 M. A. Ramírez, P. R. Bueno, J. A. Varela and E. Longo, *Appl. Phys. Lett.*, 2006, **89**, 212102.
26 J. Boonlakhorn, P. Kidkhunthod and P. Thongbai, *J. Eur. Ceram. Soc.*, 2015, **35**, 3521–3528.
27 L. Sun, R. Zhang, Z. Wang, E. Cao, Y. Zhang and L. Ju, *RSC Adv.*, 2016, **6**, 55984–55989.
28 L. Ni and X. M. Chen, *Solid State Commun.*, 2009, **149**, 379–383.
29 A. Nautiyal, C. Autret, C. Honstettre, S. De Almeida-Didry, M. El Amrani, S. Roger, B. Negulescu and A. Ruyter, *J. Eur. Ceram. Soc.*, 2016, **36**, 1391–1398.
30 M. F. Ab Rahman, S. D. Hutagalung, Z. A. Ahmad, M. F. Ain and J. J. Mohamed, *J. Mater. Sci.: Mater. Electron.*, 2015, **26**, 3947–3956.
31 L. Singh, I. W. Kim, B. C. Sin, K. D. Mandal, U. S. Rai, A. Ullah, H. Chung and Y. Lee, *RSC Adv.*, 2014, **4**, 52770–52784.
32 L. Ni and X. M. Chen, *J. Am. Ceram. Soc.*, 2010, **93**, 184–189.
33 W. L. Li, Y. Zhao, Q. G. Chi, Z. G. Zhang and W. D. Fei, *RSC Adv.*, 2012, **2**, 6073.
34 M. Gao, D. Feng, G. Yao, Y. Zhang, C. L. Chen and Y. Lin, *RSC Adv.*, 2015, **5**, 92958–92962.
35 L. Singh, B. C. Sin, I. W. Kim, K. D. Mandal, H. Chung, Y. Lee and J. Varela, *J. Am. Ceram. Soc.*, 2016, **99**, 27–34.
36 J. Boonlakhorn and P. Thongbai, *Jpn. J. Appl. Phys.*, 2015, **54**, 06FJ06.
37 R. Yu, H. Xue, Z. Cao, L. Chen and Z. Xiong, *J. Eur. Ceram. Soc.*, 2012, **32**, 1245–1249.
38 A. E. Smith, T. G. Calvarese, A. W. Sleight and M. A. Subramanian, *J. Solid State Chem.*, 2009, **182**, 409–411.
39 M. Newville, *J. Synchrotron Radiat.*, 2001, **8**, 96–100.
40 R. D. Shannon, *Acta Crystallogr., Sect. A: Cryst. Phys., Diffr., Theor. Gen. Crystallogr.*, 1976, **32**, 751–767.
41 M. Li, Z. Shen, M. Nygren, A. Feteira, D. C. Sinclair and A. R. West, *J. Appl. Phys.*, 2009, **106**, 104106.
42 S. I. R. Costa, M. Li, J. R. Frade and D. C. Sinclair, *RSC Adv.*, 2013, **3**, 7030–7036.
43 R. Schmidt, S. Pandey, P. Fiorenza and D. C. Sinclair, *RSC Adv.*, 2013, **3**, 14580–14589.
44 L. Liu, Y. Huang, Y. Li, D. Shi, S. Zheng, S. Wu, L. Fang and C. Hu, *J. Mater. Sci.*, 2012, **47**, 2294–2299.
45 J. Deng, X. Sun, S. Liu, L. Liu, T. Yan, L. Fang and B. Elouadi, *J. Adv. Dielectr.*, 2016, **06**, 1650009.
46 G. Li, Z. Chen, X. Sun, L. Liu, L. Fang and B. Elouadi, *Mater. Res. Bull.*, 2015, **65**, 260–265.
47 J. Jumpatam, A. Mooltang, B. Putasaeng, P. Kidkhunthod, N. Chanlek, P. Thongbai and S. Maensiri, *Ceram. Int.*, 2016, **42**, 16287–16295.
48 Y. Huang, D. Shi, Y. Li, G. Li, Q. Wang, L. Liu and L. Fang, *J. Mater. Sci.: Mater. Electron.*, 2012, **24**, 1994–1999.
49 L. Liu, L. Fang, Y. Huang, Y. Li, D. Shi, S. Zheng, S. Wu and C. Hu, *J. Appl. Phys.*, 2011, **110**, 094101.
50 M. Li and D. C. Sinclair, *J. Appl. Phys.*, 2013, **114**, 034106.